

# Universal temperature dependence of optical excitation life-time and band-gap in chirality assigned semiconducting single-wall carbon nanotubes

Ferenc Simon<sup>†</sup>, Rudolf Pfeiffer, and Hans Kuzmany

*Institut für Materialphysik, Universität Wien, Strudlhofgasse 4, A-1090 Wien, Austria*

The temperature dependence of optical excitation life-time,  $1/\Gamma$ , and transition energies,  $E_{ii}$ , were measured for bucky-papers of single-wall carbon nanotubes (SWCNTs) and inner tubes in double-wall carbon nanotubes (DWCNTs) using resonant Raman scattering. The temperature dependence of  $\Gamma$  and  $E_{ii}$  is the same for both types of samples and is independent of tube chirality. The data proves that electron-phonon interaction is responsible for temperature dependence of  $E_{ii}(T)$ . The temperature independent inhomogeneous contribution to  $\Gamma$  is much larger in the SWCNT samples, which is explained by the different SWCNT environment in the two types of samples.  $\Gamma$  of the inner tubes for the bucky-paper DWCNT sample is as low as  $\sim 30$  meV, which is comparable to that found for individual SWCNTs.

Single-wall carbon nanotubes (SWCNTs) have been in the focus of interest in the last decade due to their unique physical and chemical properties, which makes them a potential candidate for a broad range of applications [1, 2]. It is now established theoretically [3, 4, 5, 6] and there is emerging experimental evidence [7, 8, 9, 10] that excitonic effects, i.e. the correlation of photoexcited electrons and holes, play an important role in the optical absorption and emission properties of single-wall carbon nanotubes (SWCNTs). The life-time of the excitons,  $\tau_{\text{exciton}}$ , and the optical excitation energies,  $E_{ii}$ , and their temperature dependencies are crucial parameters for the optoelectronic applications of SWCNTs. SWCNTs are characterized by the great variation of physical properties depending on the  $(n, m)$  chiral indices. Therefore chirality assigned determination of these parameters is vital.  $\tau_{\text{exciton}}$  was measured in time-resolved photoexcited studies [11, 12, 13, 14] and estimated theoretically [15, 16].  $E_{ii}$  was measured using photoluminescence spectroscopy in a chirality assigned manner for ensembles of isolated SWCNTs [17] and for individual SWCNTs [18, 19].

The scattering rate of the optically excited states,  $\Gamma = 1/\tau$ , is related to  $\tau_{\text{exciton}}$ . Both  $\Gamma$  and  $E_{ii}$  are accessible from resonant Raman scattering (RRS) studies [20, 21]. Such studies have been presented on surfactant separated [22, 23] and also for bucky-paper SWCNT samples [22]. The temperature dependence, studied using varying laser powers, of  $E_{ii}$  was found to markedly differ for  $\nu = 1$  and  $\nu = 2$  type semiconducting SWCNTs, where  $\nu$  is given by  $(n - m) \bmod 3 = \nu$ .  $\nu = 1$  tubes were found to blue-shift whereas  $\nu = 2$  to red-shift with increasing temperature. In a recent study,  $E_{ii}$  was found to red-shift for both  $\nu = 1, 2$  with increasing temperature for individual SWCNTs [24], which was explained by the electron-phonon coupling [24, 25]. The anomalous dependence observed for bucky-paper samples in Ref. [22] is still unresolved. Clearly, the role for the tube environment requires further studies. In addition, no temperature dependent measurement of  $\Gamma$  on chirality assigned SWCNTs is available.

Here, the temperature dependence of the  $(n, m)$  spe-

cific electronic transitions and scattering rates for optical excitations is reported for SWCNTs in different environment. We measured SWCNTs with the same chirality in bucky-paper SWCNT samples and as inner tubes in double-wall carbon nanotube (DWCNT) samples. The latter type of sample has attracted considerable interest as the inner tubes are in a well-shielded environment, which results in exceptionally long phonon life-times [26, 27]. The current study explains the role of the tube environment on the two parameters studied. A carbon nanotube is surrounded by other tubes with random chiralities in an SWCNT sample, however a given inner-tube can be embedded in outer tubes with a few well defined chiralities. In addition, the narrow Raman line-widths of the inner-tubes result in distinct inner-tube Raman spectra of the studied tube-pairs [26, 28]. We indeed observe a large inhomogeneous contribution to  $\Gamma$  for the SWCNT sample but the same temperature dependence as for the inner tubes in the DWCNT. The same temperature dependence of  $E_{ii}$  was observed for both types of samples. These results suggest that both parameters are independent of the tube environment and suggest a common and robust mechanism for them.

The SWCNTs we studied were HiPco (Carbon Nanotechnologies Inc. Houston, USA) and CoMoCat samples (SouthWest NanoTechnologies Inc. Oklahoma, USA) with mean tube diameters of  $d = 1.0$  nm and  $d = 0.8$  nm, respectively as determined from a Raman analysis [21]. The DWCNTs were produced from SWCNTs encapsulating fullerenes, so-called peapods [29]. The host SWCNTs (Nanocarblab, Moscow, Russia) with a mean diameter of 1.40 nm were sealed under vacuum in a quartz tube together with the  $C_{60}$  powder and heated at 650 °C for 2 hours [30]. The resulting peapods were annealed in dynamic vacuum at 1270 °C for 2 hours which results in DWCNTs [26, 31]. The inner tube diameter distribution follows that of the outer tube [32, 33] and we obtained  $d = 0.7$  nm for the mean diameter from a Raman analysis [33]. As a result, the diameter distribution of SWCNTs and inner tubes are very similar for the three samples.

Raman spectroscopy was performed on a Dilor xy

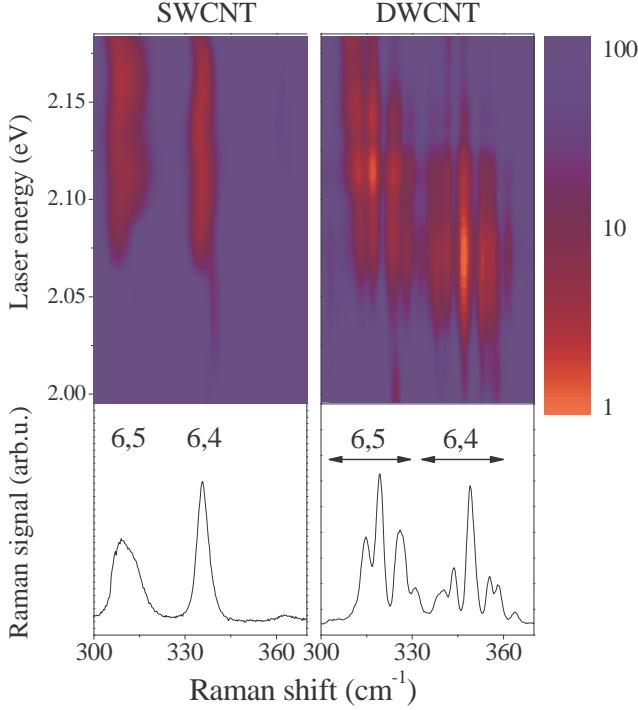


FIG. 1: *Color online* Energy dispersive Raman contour plot for SWCNT(CoMoCat) and DWCNT samples at 80 K. The vertical bar shows the color coding for the observed intensities on a logarithmic scale in arbitrary units. Lower panels show individual Raman spectra with 2.10 eV laser energy.

triple grating instrument equipped with a home-built cryostat for the 80-600 K temperature range. The excitation was provided by a tunable laser in the 2.01-2.18 eV (616-568 nm) energy range involving 22 different laser energies. A series of discharge calibration lamps and Si powder were used to calibrate the Raman shifts and the Raman intensities, respectively. The samples were mounted on the cold finger of a liquid nitrogen cooled cryostat with conducting silver for good thermal contact. The spectrometer was operated in the "macro" acquisition mode with typical laser power densities of 5 mW/(100  $\mu\text{m}$ )<sup>2</sup> to avoid sample heating.

In Fig. 1 we show the energy dispersive Raman map for the SWCNT(CoMoCat) and DWCNT samples for a part of the radial breathing mode (RBM) and excitation energy range at 80 K. Similar contour plots showing a larger area, have been used to assign  $(n, m)$  indexes to the different nanotubes in SWCNT [22, 23] and DWCNT samples [34]. The two peaks at 310 and 337  $\text{cm}^{-1}$  with 2.12 and 2.08 eV transition energies correspond to the  $E_{22}$  optical transition enhanced RBMs of the (6,5) and (6,4) tubes for the SWCNT sample [22, 23]. These two tubes are representative for both semiconducting SWCNT classes  $\nu = 1$  and  $\nu = 2$  and their RBMs are well separated from all other tube modes. This renders them ideal for studying the temperature dependent RRS. For the DWCNT,

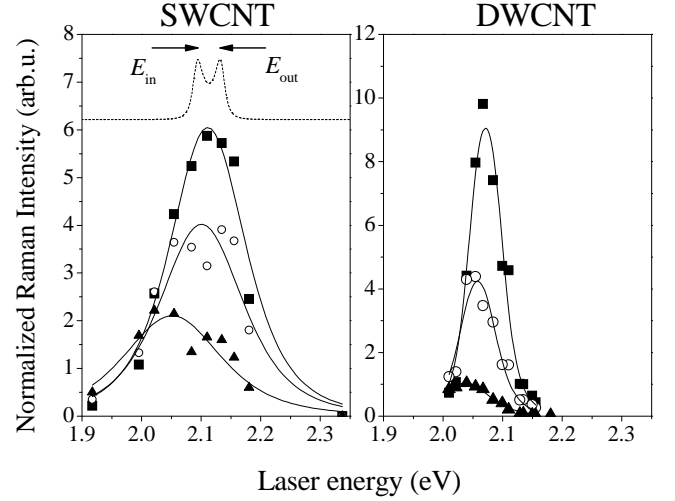


FIG. 2: Raman resonance profile for the (6,4) tubes in the SWCNT (CoMoCat) and DWCNT samples,  $\blacksquare$ : 80 K,  $\circ$ : 300 K,  $\blacktriangle$ : 600 K. Solid curves show fits with the RRS theory. Dashed curve is a simulation for the 80 K SWCNT data with  $\Gamma = 10$  meV. Arrows indicate the incoming and outgoing resonance energies. Note the much narrower widths for the DWCNT sample.

(6,5) and (6,4) are inner tubes and their RBMs are split into several components as the same inner tube can be in several outer ones [34, 35]. The difference in the resonance energies results from the different environment for the two samples: an outer tube for the DWCNT sample and the surrounding ensemble of the other SWCNTs for the SWCNT sample. The gradual red-shift for the inner tube resonance energies with increasing Raman shift was associated to the pressure induced by the outer tubes [34].

The temperature dependence of the Raman contour plots was measured for all three samples. Raman intensities corresponding to individual modes were determined by fitting Voigtian line-shapes whose Gaussian component was given by the residual spectrometer resolution. The energy dependent Raman intensities for two particular tube modes in the two kinds of samples are shown in Fig. 2 as a function of temperature. For the SWCNT CoMoCat sample the (6,4) tube mode at 337  $\text{cm}^{-1}$  (phonon energy  $E_{\text{ph}} = 41.8$  meV) is shown and the strongest (6,4) inner tube component at 347  $\text{cm}^{-1}$  ( $E_{\text{ph}} = 43$  meV) is shown for the DWCNT sample. The temperature dependent resonant Raman data can be fitted with the resonance Raman theory for Stokes Raman modes [20, 21]:

$$I(E_l) = M_{\text{eff}}^4 \left| \frac{(E_l - E_{\text{ph}})^4 (n_{\text{BE}}(E_{\text{ph}}) + 1)}{(E_l - E_{\text{ii}} - i\Gamma)(E_l - E_{\text{ph}} - E_{\text{ii}} - i\Gamma)} \right|^2 \quad (1)$$

Here, the electronic density of states of SWCNTs is assumed to be a Dirac function and the effective matrix element,  $M_{\text{eff}}$ , describing the electron-phonon interac-

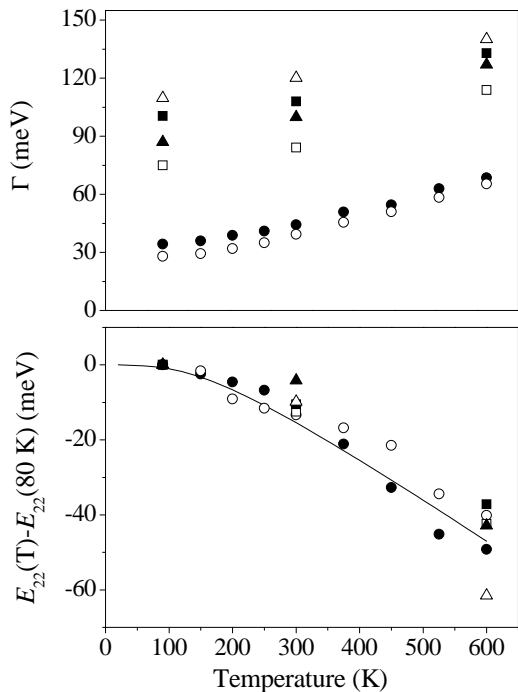


FIG. 3: Temperature dependence of the optical transition energy shift,  $E_{22}(T) - E_{22}(80 \text{ K})$ , and the damping parameter,  $\Gamma$  for the (6,5) and (6,4) inner tubes of DWCNTs, HiPco tubes, and CoMoCat tubes. Open and closed symbols are for the (6,4) and (6,5) tubes, respectively.  $\triangle$ : CoMoCat,  $\square$ : HiPco,  $\circ$ : DWCNT. Solid curve is a calculation for the red-shifting  $E_{22}$  for a (6,5) tube as explained in the text.

tions is taken to be independent of temperature and energy.  $E_l$ ,  $E_{22}$  and  $E_{ph}$  are the exciting laser, the optical transition and the phonon energies, respectively.  $n_{BE}(E_{ph}) = (\exp(E_{ph}/k_B T) - 1)^{-1}$  is the Bose-Einstein function and accounts for the thermal population of the vibrational state [36] and  $n_{BE}(E_{ph}) + 1$  changes a factor  $\sim 2$  between 80 and 600 K. The temperature dependence of  $E_{ph}$  is  $\sim 1\%$  for the studied temperature range [37] thus it can be neglected. The first and second terms in the denominator of Eq. 1 describe the incoming and outgoing resonances, respectively and are indicated on a simulated curve by arrows in Fig. 2. These are separated by  $E_{ph}$ . This means the apparent width of the resonance Raman data does not represent  $\Gamma$ .

Solid curves in Fig. 2 show fits for the data at all temperatures simultaneously using Eq. 1 and allow thus to derive the temperature dependence for  $E_{22}$  and  $\Gamma$ . The simultaneous fit improves its reliability compared to fitting separately to the particular temperatures such as in Ref. [24]. The result for the temperature dependent relative optical transition energies,  $E_{22}(T) - E_{22}(80 \text{ K})$  and  $\Gamma(T)$  is summarized in Fig. 3. The room temperature values of  $E_{22}$  is given in Table I together with the  $\Gamma(80 \text{ K})$  and the  $\Delta\Gamma = \Gamma(600 \text{ K}) - \Gamma(80 \text{ K})$  parameters for the three samples studied.

TABLE I: Transition energies,  $E_{22}$ , and the damping parameter,  $\Gamma$  in the two SWCNT and the DWCNT samples. The HiPco sample dispersed in SDS were studied at room temperature in Ref. [22]. Relative errors are  $2 \cdot 10^{-3}$  for  $E_{22}$  and 0.1 for  $\Gamma$ .

	$E_{22}$ (eV)		$\Gamma(80 \text{ K})$ (meV)		$\Delta\Gamma$ (meV)	
	(6,5)	(6,4)	(6,5)	(6,4)	(6,5)	(6,4)
CoMoCat	2.12	2.08	90	109	40	31
HiPco	2.11	2.07	100	77	33	38
HiPco SDS [22, 38]	2.18	2.11	35	35	—	—
DWCNT	2.09	2.04	34	27	34	38

We start the discussion with the  $T$  dependent optical transition energies. Differences between the room temperature values for  $E_{22}$ 's for DWCNT [34], SWCNT in bucky-paper and as dispersed [22] have been previously observed and explained by the effect of the different environment. The surprising observation is the overall red-shift of 50(10) meV between 80 and 600 K irrespective of the sample type and the family of tube,  $\nu = 1$  or 2. Recently,  $\sim 50$  meV red-shifts were observed for individual suspended nanotubes using the same method for SWCNTs with  $\nu_{RBM} > 250 \text{ cm}^{-1}$  [24]. The observed temperature dependence was explained by the softening of the band gap at high temperatures due to electron-phonon coupling [24, 25] yielding the optical transition energy shift:

$$\Delta E_{22}(T) = \alpha_1 \Theta_1 n_{BE}(k_B \Theta_1) + \alpha_2 \Theta_2 n_{BE}(k_B \Theta_2) \quad (2)$$

In Fig. 3, we show the calculated  $\Delta E_{22}(T)$  using Eq. 2 with  $\alpha_1 = -1.17 \cdot 10^{-5} \text{ eV/K}$ ,  $\alpha_2 = -1.04 \cdot 10^{-4} \text{ eV/K}$ ,  $\Theta_1 = 103.8 \text{ K}$ , and  $\Theta_2 = 487.4 \text{ K}$  for a (6,5) tube from Ref. [24]. Since  $\Delta E_{22}(80 \text{ K}) \approx \Delta E_{22}(0 \text{ K})$  plotting  $\Delta E_{22}(T)$  on the  $E_{22}(T) - E_{22}(80 \text{ K})$  data is justified. A similar calculation for a (6,4) tube does not give a significantly different curve. A good agreement between the experimental points and the calculation is observed, which confirms the validity of the theoretical explanation presented in Ref. [25]. Both ours and the results in Ref. [24] are in difference to a previous study in which a blue-shift with increasing temperature was reported for  $\nu = 1$  tubes in a laser heated sample [22]. Since the current experimental conditions provide a reliable control over the true sample temperature the samples studied here behave differently as compared to those studied previously.

Our result confirms the red-shift of optical transition energies with increasing temperature as observed on individual tubes [24]. It holds for SWCNTs in bucky-papers and for inner tubes surrounded by outer tubes in DWCNT samples. It thus unambiguously proves that electron-phonon interaction is the dominant mechanism for the temperature variation of the optical transitions and other effects such as thermal expansion, proposed in

Ref. [24] do not play a role.

The temperature dependent  $\Gamma(T)$  can be separated into a residual and a  $T$  dependent part. The measurement for the lowest temperatures, the  $\Gamma(80\text{ K})$  values, approximate the residual  $\Gamma_0$  which shows marked differences for the three samples. In contrast the change with temperature,  $\Delta\Gamma = \Gamma(600\text{ K}) - \Gamma(80\text{ K})$ , is similar for all samples and chiralities studied and scatters in the 20-30 meV range. We assign the temperature dependent part of  $\Gamma(T)$  to homogeneous thus to a true life-time effect and the residual  $\Gamma_0$  to inhomogeneous broadening.

The low value of  $\Gamma_0$  for individual SDS dispersed SWCNTs and inner tubes in DWCNTs and its high value for the two bucky-paper samples of SWCNTs can be explained by the sample morphologies assuming that nearest neighbor tube-tube interactions strongly affect the transition energies. For the bucky-paper SWCNT samples, each tube is surrounded by other tubes with random chiralities. The interaction between the tubes gives rise to a distribution of transition energies, which appears as an inhomogeneous broadening of the RRS. For individual SWCNTs the environment is the same for all tubes, thus transition energies are well defined. For inner tubes in the DWCNT bucky-paper sample, an inner tube can be embedded in outer tubes with several possible chiralities [34, 35]. However these inner-outer tube pairs are well resolved spectroscopically for most of the inner tubes and in particular for the (6,5) and (6,4) tubes studied. Thus the inner tube transition energies are well defined for each inner-outer tube pair and  $\Gamma$  is not affected by inhomogeneous effects.

The current data for  $\Gamma$  also account for the observation of the extremely large Raman cross section of inner tubes as compared to SWCNTs [26, 28, 39]. The factor two smaller  $\Gamma$  of inner tubes results in an approximate enhancement of a factor 16 in the Raman cross section as the latter is proportional to  $\left(\Gamma^2 \left(E_{\text{ph}}^2 + \Gamma^2\right)\right)^{-1}$ .

In conclusion, we studied the temperature dependent resonant Raman scattering on small diameter SWCNTs and inner tubes in DWCNTs. An overall red-shift of the optical transition energies with the same magnitude irrespective of tube type was observed. We observed the same  $T$  dependence of the inverse optical excitation lifetime,  $\Gamma$ , which is attributed to fundamental on-the tube scattering mechanisms. The environment gives rise to an inhomogeneous broadening of the RRS resonance profiles and results in a small  $\Gamma$  for the inner tubes. Interestingly,  $\Gamma$  for inner tubes in a bucky-paper sample of DWCNTs is identical for a micelle-suspended SWCNTs. Thus the current result underlines the application potential of DWCNTs in future optoelectronic devices. The measurement of the temperature dependence of  $\Gamma$  and of the optical transition energies provides important input for theories explaining the optical properties of carbon nanotubes.

Supported by the FWF project Nr. 17345 and by the EU Grants MERG-CT-2005-022103 and BIN2-2001-00580. F.S. acknowledges the Zoltán Magyary post-doctoral programme and the Hungarian State Grants (OTKA) No. TS049881, F61733 and NK60984 for support.

†corresponding author: ferenc.simon@univie.ac.at  
Present address: Budapest University of Technology and Economics, Institute of Physics and Solids in Magnetic Fields Research Group of the Hungarian Academy of Sciences, H-1521, Budapest P.O.Box 91, Hungary

- 
- [1] R. Saito, G. Dresselhaus, and M. Dresselhaus, *Physical Properties of Carbon Nanotubes* (Imperial College Press, 1998).
  - [2] M. S. Dresselhaus, G. Dresselhaus, and P. Avouris, *Carbon Nanotubes: Synthesis, Structure, Properties, and Applications* (Springer, 2001).
  - [3] C. L. Kane and E. J. Mele, Phys. Rev. Lett. **90**, 207401 (2003).
  - [4] C. D. Spataru *et al.*, Phys. Rev. Lett. **92**, 077402 (2004).
  - [5] V. Perebeinos, J. Tersoff, and P. Avouris, Phys. Phys. Lett. **92**, 257402 (2004).
  - [6] V. Perebeinos, J. Tersoff, and P. Avouris, Phys. Phys. Lett. **94**, 027402 (2005).
  - [7] F. Wang *et al.*, Science **308**, 838 (2005).
  - [8] J. Maultzsch *et al.*, Phys. Rev. B **72**, 241402(R) (2005).
  - [9] F. Plentz *et al.*, cond-mat/0507104.
  - [10] Y. Miyauchi and S. Maruyama, cond-mat/0508232.
  - [11] J.-S. Lauret *et al.*, Phys. Rev. Lett. **90**, 57404 (2003).
  - [12] F. Wang *et al.*, Phys. Rev. Lett. **92**, 177401 (2004).
  - [13] G. N. Ostojic *et al.*, Phys. Rev. Lett. **92**, 117402 (2004).
  - [14] A. Hagen *et al.*, Phys. Rev. Lett. **95**, 197401 (2005).
  - [15] C. D. Spataru *et al.*, Phys. Rev. Lett. **95**, 247402 (2005).
  - [16] V. Perebeinos, J. Tersoff, and P. Avouris, Nano Lett. **5**, 2495 (2005).
  - [17] S. M. Bachilo *et al.*, Science **298**, 2361 (2002).
  - [18] J. Lefebvre *et al.*, Phys. Rev. Lett. **90**, 217401 (2003).
  - [19] A. Hartschuh *et al.*, Science **301**, 1354 (2003).
  - [20] R. M. Martin and L. M. Falicov, *Resonant Raman Scattering* (Springer, Berlin, 1983), p. 79.
  - [21] H. Kuzmany *et al.*, Eur. Phys. J. B **22**, 307 (2001).
  - [22] C. Fantini *et al.*, Phys. Rev. Lett. **93**, 147406 (2004).
  - [23] H. Telg *et al.*, Phys. Rev. Lett. **93**, 177401 (2004).
  - [24] S. B. Cronin *et al.*, et al., Phys. Rev. Lett. **96**, 127403 (2006).
  - [25] R. B. Capaz *et al.*, Phys. Rev. Lett. **94**, 036801 (2005).
  - [26] R. Pfeiffer *et al.*, Phys. Rev. Lett. **90**, 225501 (2003).
  - [27] F. Simon *et al.*, Chem. Phys. Lett. **413**, 506 (2005).
  - [28] R. Pfeiffer *et al.*, Phys. Rev. B **71**, 155409 (2005).
  - [29] B. W. Smith, M. Monthieux, and D. E. Luzzi, Nature **396**, 323 (1998).
  - [30] H. Kataura *et al.*, Synthetic Met. **121**, 1195 (2001).
  - [31] S. Bandow, M. Takizawa *et al.*, Chem. Phys. Lett. **337**, 48 (2001).
  - [32] M. Abe *et al.*, et al., Phys. Rev. B **68**, 041405(R) (2003).
  - [33] F. Simon *et al.*, Phys. Rev. B **71**, 165439 (2005).
  - [34] R. Pfeiffer *et al.*, Phys. Rev. B **72**, 161404(R) (2005).
  - [35] R. Pfeiffer *et al.*, Eur. Phys. J. B **42**, 345 (2004).

- [36] H. Kuzmany, *Solid-State Spectroscopy, An Introduction* (Springer, 1998).
- [37] N. R. Raravikar *et al.*, Phys. Rev. B **66**, 235424 (2002).
- [38] Values of  $\Gamma$  with a factor two larger are given in Ref. [22] which was admitted to result from an error in the resonance analysis.
- [39] F. Simon *et al.*, Phys. Rev. Lett. **95**, 017401 (2005).